Journal of Catalysis **210,** 84–96 (2002)
doi:10.1006/jcat.2002.3666

The Effect of Water on the Cobalt-Catalyzed Fischer–Tropsch Synthesis

Christopher J. Bertole,* Charles A. Mims,*,[1] and Gabor Kiss†,[1]

*Department of Chemical Engineering and Applied Chemistry, University of Toronto, Toronto, Ontario, Canada M5S3E5; and †ExxonMobil Research and Engineering Company, Corporate Strategic Research, 1545Route 22E, Annandale, New Jersey 08801

Received December 11, 2001; revised April 30, 2002; accepted May 8, 2002

Carbon isotope transients at reaction steady state are used to examine the effect of water vapor on the amount and reactivity of the surface carbon intermediates involved in the Fischer–Tropsch synthesis on both a supported and an unsupported cobalt catalyst. Water increases the amount of active surface carbon, present predominantly as monomeric species. This increased surface concentration of monomeric carbon is caused by an acceleration of the CO dissociation rate without a matching reactivity increase in the downstream hydrocarbon synthesis steps. In turn, the proposed monomer dependencies in the Fischer–Tropsch synthesis mechanism explain the lower methane selectivity and higher molecular weight products observed at increased water concentrations.

Key Words: **Fischer–Tropsch synthesis; cobalt catalyst; water effect; isotope transient.**

INTRODUCTION

Cobalt-catalyzed Fischer–Tropsch (FT) synthesis produces water along with the desired hydrocarbon products. At the conditions reached in commercial practice, large water concentrations are present. Water vapor has been shown to influence the performance of cobalt FT catalysts in a variety of ways. Both reversible kinetic effects as well as irreversible changes to the catalyst have been associated with water. For example, it was observed that water reversibly enhances the activity of some cobalt catalysts but not all (1–10). In some cases (5, 10) even rate-inhibiting effects are mentioned. Kim (7, 8) observed that reversible activity enhancement by water addition only occurs on catalysts with low-surface-area, large-pore-radius supports. It has been proposed that condensation of an aqueous phase in the pores assists mass transport in some catalysts (1, 3), while it has been suggested that water's ability to affect the degree of surface decoration by support-derived species plays a role in other cases (1). Despite these demonstrated effects, water terms generally do not appear in published reaction rate laws for cobalt catalysts (11, 12) nor do they appear in inhibiting terms (5); however, the beneficial effects of water addition are recognized in various patents (6–9).

Reversible selectivity changes induced by water include decreased methane selectivity, higher product olefinicity at a given carbon number, and an increased fraction of higher molecular weight products (1–4, 6–9, 13). Water also mildly affects the production of branched hydrocarbons and internal alkene isomers (9). Water-induced selectivity changes have been attributed to suppression of the hydrogenation activity of the metal surface, presumably by competitive adsorption (1, 13). This effect decreases both methane selectivity and the hydrogenation of alkenes, the latter supposedly leading in turn to a higher probability of olefin readsorption and further growth (1). As detailed in Ref. (1), the reversible effects of water on catalyst activity and selectivity are not well understood, and there is no single, simple explanation for all of the observations.

The irreversible effects of high water pressure on cobalt catalysts generally involve the loss of activity (13–24). These irreversible effects also have multiple proposed explanations. For example, small cobalt particles may reoxidize at high water pressures (13–15, 17–22). Also, interactions between cobalt and the support can be facilitated by water, even to the point of mixed oxide formation (13, 14, 17, 23, 24). Holmen and co-workers (18, 19) used isotope transients to show that exposure of alumina-supported cobalt catalysts to water-containing syngas feeds decreases the number of active sites without a loss of site activity. Deactivation is reportedly more severe in the presence of Re promoter (17).

In this study, we apply transient isotope techniques at reaction steady state with and without the presence of water in the feed to better understand the kinetic effects of water. As mentioned before, cobalt-support interactions are facilitated by the presence of water leading to deactivation (13–24). These deactivation processes significantly complicate the separation of reversible kinetic effects and irreversible deactivation. In order to eliminate the complications caused by possible support effects, we use an unsupported cobalt catalyst in most of the reported experiments and thus isolate the kinetic effects of water on the active cobalt surface. A titania-supported catalyst is also used to determine whether

[1] To whom correspondence should be addressed. E-mail: MIMS@CHEM-ENG.UTORONTO.CA, gabor.kiss@exxonmobil.com.

0021-9517/02 $35.00

the presence of a support influences the kinetic and selectivity responses to added water.

Isotope transient investigations of the effects of water on FT synthesis have until now been limited to examinations of the catalyst after steam exposure, but those experiments do not shed light on the reversible, kinetic effects of water (18, 19). Our studies overcome these limitations by investigating elevated-pressure, water-containing reaction conditions encountered in commercial practice.

Isotope transients at reaction steady state (also referred to as SSITKA (25)) reveal the amount and residence-time distribution of species containing the labeled atom on the catalyst. The use of a ^{12}CO–^{13}CO transient in the feed has been used many times to investigate FT synthesis (18, 19, 25–34). It reveals both the inventory of reversibly adsorbed CO and the residence time distribution of the carbon-containing intermediates destined to become hydrocarbon products. By providing an *in situ* probe of the steady state catalytic processes, it can immediately distinguish changes in the number of sites from changes in site activity.

Previous isotope transient studies of FT synthesis at low pressures have revealed that working Ru and Co catalysts contain essentially a monolayer of reversibly adsorbed CO (31, 32). They also revealed that the majority of the active carbon intermediates at steady state are monomeric precursors to the hydrocarbon products (26, 32, 56). Therefore, the flow of carbon relevant to its residence time on the surface can be approximately represented by the scheme in Fig. 1, which involves two essentially irreversible steps on the surface after CO adsorption. In the first step, adsorbed CO reacts to form C*, the active carbon monomer species, the precursor to all hydrocarbons. In the second step, C* is converted to products by means of a complex network of reactions, lumped into a single step in Fig. 1. We assign both these steps a pseudo-first-order rate coefficient. Thus, at steady state the rate of conversion of adsorbed CO to the active carbon pool, C*, is equal to the CO conversion rate, r_{CO}, and is given by

$$r_{CO} = k_{CO}\theta_{CO}. \quad [1]$$

In this instance, the conversion rate, r_{CO}, is written as the site turnover frequency, while θ_{CO} is the fractional site coverage by CO, and k_{CO} is the pseudo-first-order rate coefficient of converting adsorbed CO into C*. The rate on a cobalt metal basis, r'_{CO} (in moles of CO per mole of cobalt per second), is simply given by multiplying r_{CO} by the number of sites

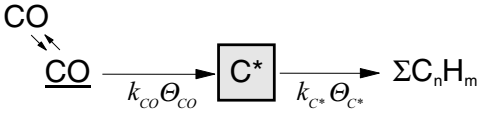

FIG. 1. Simplified kinetic scheme for the carbon reaction pathways in FT synthesis on cobalt.

per mole of cobalt atom (N_S/N_{Co}). We later equate N_S with N_{CO}, the amount of adsorbed carbon monoxide at reaction steady state.

At steady state, the conversion rate of C* to the final product slate is also equal to r_{CO} and in the simplest analysis can also be assigned a pseudo-first-order rate coefficient, k_{C^*}:

$$r_{CO} = r_{C^*} = k_{C^*}\theta_{C^*}. \quad [2]$$

In this case the rate coefficient, k_{C^*}, represents the entire hydrocarbon synthesis network and it contains a complex dependence on the steady state amounts of many surface species, including H*, *OH, open sites, and others. θ_{C^*} is the fractional site coverage of the active metal by the active carbon monomer species.

The steady state amount of exchangeable adsorbed CO, proportional to θ_{CO}, is directly measured by the ^{12}CO–^{13}CO isotope transients. Since all hydrocarbon products arise virtually instantaneously from a common pool of monomeric carbon (26, 32), the kinetics of C* removal can be measured in any of the products. Methane, in addition to being easily measured by mass spectrometry, is also the least susceptible of the hydrocarbon products to further holdup in the reactor due to mass transport or high solubility in the resident liquid product. For these reasons, we rely on the methane transients in the assessment of the C* residence time (τ_{C^*}). The reciprocal of τ_{C^*} directly yields the pseudo-first-order rate constant for C* conversion, k_{C^*}, and thus can also be obtained independently of other kinetic parameters.

The amount of isotope in the washout curve of the products during an isotopic transient is a true measure of the surface coverage at steady state if the conversion processes are irreversible and no exchange occurs with other reservoirs of carbon. In addition, examining the shape of the isotope transient in the products can assess the validity of the pseudo-first-order approximation in Eq. [2]. If the monomer is a homogeneous pool of a single intermediate, the isotope washout curve should be a single exponential decay (31).

It is clear from the simple model above that the steady state concentration of active carbon on the surface, θ_{C^*}, is governed by a dynamic balance between its formation by CO activation and its removal in the hydrocarbon synthesis process. Thus, for example, an increase in the CO activation rate (k_{CO}) without a parallel increase in C* reactivity (k_{C^*}) and without changing the CO coverage (θ_{CO}) will increase the surface coverage of C* at steady state, since from Eqs. [1] and [2]

$$\theta_{C^*}/\theta_{CO} = k_{CO}/k_{C^*} \quad [3]$$

In a previous study comparing various catalysts at a single reaction condition (35), we observed that catalysts with lower methane selectivity tended to have a higher surface coverage of active carbon. Such a trend naturally occurs

if higher hydrocarbon formation (i.e., C* polymerization) kinetics follow a higher effective order in surface carbon concentration than does methane formation. This assumption is imbedded in simple FT polymerization mechanisms, and in Ref. (35), we showed that this bias alone could explain the observed correlation of selectivity with carbon coverage. Our present results show that water has a dramatic effect on the dynamic balance surrounding C*: water increases the C* coverage by preferentially increasing the rate of CO activation, i.e., the rate of C* production, over the rate of C* conversion leading to a buildup of C*. In our discussion of these results, we show that the same selectivity bias with carbon coverage described in Ref. (35) can also explain the shift in product selectivity seen upon water addition.

EXPERIMENTAL

We used both a titania-supported cobalt catalyst (in the following discussion referred to as titania-supported cobalt, or Co–Re/TiO_2) and an unsupported cobalt catalyst (referred to as unsupported cobalt, or Co–Re). Rhenium promotion was used in the supported catalyst to enhance cobalt dispersion and the reduction of Co_3O_4 (36). We also used Re in the unsupported cobalt sample. We should mention that our previous study (37) showed that the presence of rhenium affects neither the steady state catalyst performance nor the isotope transient behavior. As discussed earlier, most of the results were obtained with the unsupported catalyst to eliminate the possibility of cobalt-support interactions. The unsupported catalyst was chosen as a primary test system in order to isolate the intrinsic kinetic effects of water addition from other potential confounding issues, such as potential cobalt-support interactions and mass transfer. Table 1 lists the characteristics of the two catalysts used in our experiments.

The catalysts were tested in two distinct down-flow tubular (4-mm ID) transient reactors equipped with online mass spectrometers (MS) and gas chromatographs (GC). One reactor, described previously in (37, 38), is capable of 7 bar total pressure and was used for the supported catalyst experiments. The length of the catalyst bed in this reactor was approximately 20 mm. A newer unit, similar in design, was used for the unsupported catalyst experiments. The latter reactor is capable of operating up to 28 bar total pressure and has improved product characterization capabilities, e.g., FID analysis up to C10 hydrocarbons. The length of the catalyst bed was approximately 10 mm. Reaction temperatures were measured in both reactors by a 1/16″ thermocouple positioned in the center of the catalyst bed.

TABLE 1

Characteristics of the Cobalt Catalysts Tested

Characteristic	Catalyst	
	Unsupported Co–Re	Co–Re/TiO_2
Mass fraction Co (reduced)	0.97	0.11
Re/Co (mol/mol)	0.03	0.03
N_{CO}/N_{Co} from CO isotope transients	0.0030	0.0380

The supported (0.20 g, $<75\ \mu$m) and unsupported (0.30 g, $\approx 2\ \mu$m) catalyst samples were diluted with TiO_2 (0.15 g, rutile, 60–150 mesh) and SiC (0.23 g, Strem, 100 mesh), respectively, to assure isothermality. Both catalysts were reduced under flowing hydrogen at ambient pressure while the temperature was raised at 0.4°C/s to either 375°C (36, 37) for the supported catalyst or 250°C for the unsupported catalyst. Both catalysts were held at their final reduction temperatures for 1 h and 12.5 h, respectively, and then cooled. Syngas feed was introduced when the reactor reached 200°C and then the temperature was slowly (approximately 1°C/min) raised to the final synthesis temperature. The catalyst was on syngas for at least 20 h before rate measurements and isotope transients were performed. A backpressure regulator on the bed outlet was used to adjust the total pressure in the reactor.

CO conversions were determined by GC–MS from mass balances based on a premixed Ne internal standard. By adjusting the space velocity, the CO conversion was held in all cases to $11 \pm 2\%$. Online GC measured the C_1–C_8 (Co–Re) and C_1–C_4 (Co/TiO_2) hydrocarbon production rates. Steam was fed by adding the required amount of extra hydrogen and a stoichiometric amount of oxygen to the hydrogen stream and contacting this mixture with a heated Pt catalyst just prior to mixing with the CO/tracer stream. After each change in the reaction condition, the reaction was allowed to reach steady state (usually 1–2 h) and then run for anoth 1–2 h before another isotopic transient experiment was performed. The isotope transients were performed by switching ^{13}CO/Ar for ^{12}CO/Ne in the feed (a fixed-volume loop contained the isotope-labeled CO). Online MS followed the transient responses for methane, CO, and the tracers from the CO/tracer streams.

Only a brief examination of the effects of water was performed on the supported catalyst. The unsupported cobalt catalyst was used in a more extensive investigation over a wide range of reaction conditions at elevated pressure (39). Isotope transients and reaction kinetic data were collected for a sequence of reaction conditions without water cofeeding followed by a smaller set of experiments with cofed water. A typical isotope transient trace is shown in Fig. 2. Since measured reaction parameters and selectivity are affected by reaction conditions, periodic returns to a standard condition (210°C, $P(H_2) = 10$ bar, $P(CO) = 5$ bar,

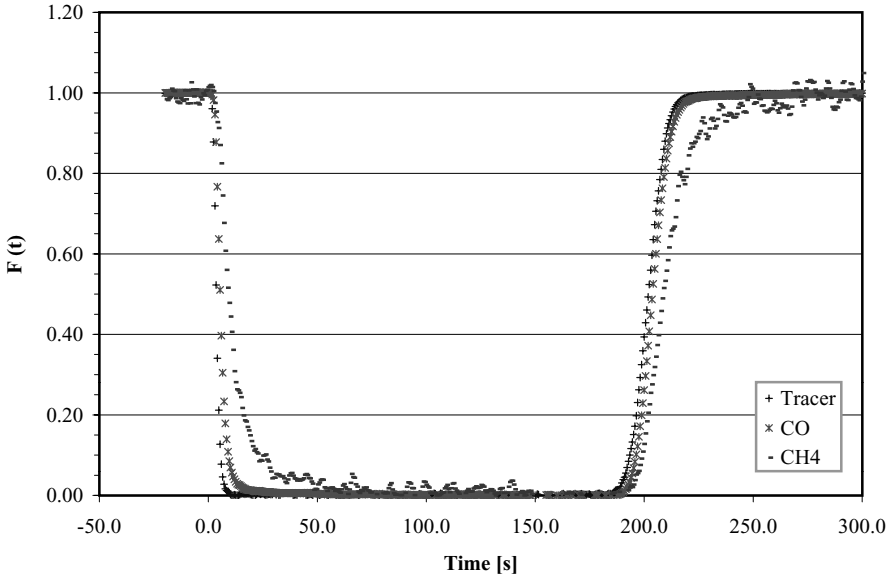

FIG. 2. Typical ^{12}C isotope transients observed after $^{12}C \rightarrow {}^{13}C \rightarrow {}^{12}C$ switches in Fischer–Tropsch synthesis at 2 MPa total pressure with the unsupported cobalt catalyst.

P(inert) = 8 bar, CO conversion = 0.10 ±0.01) were used to track irreversible changes in the catalyst.

The isotope transients provide the amount of reversibly adsorbed CO on the catalyst, N_{CO}, directly from the CO washout of the old C isotope. The moles of active carbon reporting to methane, $N_{C^*}(CH_4)$, is measured directly from the isotope washout in methane. The total amount of active carbon on the catalyst, N_{C^*}, is then calculated by

$$N_{C^*} = N_{C^*}(CH_4)/S(CH_4), \quad [4]$$

where $S(CH_4)$ is the converted CO-based methane selectivity. The pseudo-first-order rate coefficients, k_{CO} and k_{C^*}, are given by

$$k_x = R_x/N_x, \quad x = \text{CO or } C^*, \quad [5]$$

where R_x denotes the overall CO conversion rate in moles per second. k_{C^*} is obtained independently as $1/\tau_{C^*}$. It should also be recognized that

$$R_x = k_x N_x = r_x N_x/\theta_x = r_x N_S, \quad x = \text{CO or } C^* \quad \text{and} \quad N_S = \text{number of active sites.} \quad [6]$$

In our high-pressure experiments, the amount of reversibly adsorbed CO was virtually saturated and thus constant under all relevant reaction conditions. For this reason, we equate the number of active cobalt sites, N_S, in this paper to the number of reversibly adsorbed CO molecules, N_{CO}, under reaction conditions. Since by definition N_{CO} equals N_{Co}, θ_{CO} becomes equal to one. A further consequence of our site-counting method is that the CO conversion rate r_{CO} in Eq. [1] is numerically the same as the first-order rate constant k_{CO}.

The *in situ* measured "chemisorption" (i.e., the exchangeable CO values) should provide a more accurate measure of the number of active sites than *ex situ* characterization methods, such as microscopy, chemisorption, and X-ray diffraction. It is known, for example, that the number of metal sites may change in FT due to surface oxidation, mixed oxide formation, and so forth (vide supra). These changes are always accounted for by our *in situ* measurements while the same is not true when using *ex situ* methods.

We need to point out that the above-described site-counting method is not absolute. It was chosen because the isotope transients seem to provide a sensible and convenient *in situ* measure of the number of available cobalt sites despite uncertainties regarding adsorption site requirements (40). The underlying assumption of our site-counting method is that the exchangeable CO inventory is proportional to the number of active sites under reaction conditions. The exact exchangeable CO/active site ratio is not known, and we are unaware of any method that has been proven to count the true number of active sites in Fischer–Tropsch synthesis. As shown below, the *in situ* adsorbed CO inventory is almost completely independent of operating conditions, indicating that the surface capacity for CO is saturated. Thus we choose a ratio of one in our calculations without invoking full coverage of all surface cobalt sites by CO. This assumption, however, does not affect the reported trends and does not change our conclusions.

RESULTS

Titania-Supported Catalyst

Table 2 shows, in chronological order, the results of a water cofeeding and two reference dry experiments on the titania-supported catalyst. A relatively low syngas pressure ($P(H_2) = 1.1$ bar and $P(CO) = 0.55$ bar) was used with 2 bar of steam added. The water cofeed (wet) experiment was bracketed by experiments at the relevant dry condition, where inert gas was substituted for water. The kinetic parameters from the two dry experiments are identical within experimental error, showing that the effects of water are fully reversible under these conditions. The kinetic changes caused by water cofeeding in this experimental sequence are summarized in the lower portion of the table, where the wet/dry ratios of key kinetic parameters are listed. The following effects of water addition are evident.

1. The surface inventory of CO, N_{CO}, is essentially unchanged. Apparently, water does not compete effectively for the CO adsorption sites under these conditions.
2. The inventory of active surface carbon, N_{C^*}, increases by approximately 50%. The fact that the C* inventory changes substantially without an apparent effect on N_{CO} suggests that adsorbed CO and C* occupy different Co sites.
3. The CO reaction rate, r'_{CO}, expressed in the table on a cobalt metal basis, increases by approximately 50%. The first-order rate coefficient, k_{CO}, also increases by the same factor since the surface inventory of CO is not affected.
4. The reactivity of surface carbon, k_{C^*}, is essentially unaffected. The shape of the measured methane transients deviates only mildly from a single exponential decay, signifying a reasonably homogeneous pool of carbon intermediates.
5. The substantial changes in selectivity seen in the presence of water are similar to previously published results (1, 2, 13). Thus, C_{4+} selectivity increases, methane selectivity decreases, the alkene fraction in the C_2 products increases, and a small amount of CO_2 is formed by water–gas shift.

TABLE 2

Kinetic and Selectivity Results for Co–Re/TiO_2 Catalyst

Feed partial pressures[a]	1 : 0.5 : 0	1 : 0.5 : 2	1 : 0.5 : 0
CH_4 selectivity[b,c]	0.24	0.10	0.26
CO_2 selectivity[b,c]	<0.005	0.033	<0.005
C_{4+} selectivity[b,c]	0.62	0.81	0.60
Ethene fraction in C_2	0.092	0.387	0.098
r'_{CO}[c] (μmol CO/mol Co s^{-1})	680	1100	650
N_{CO}/N_{Co}	0.038	0.038	0.034
k_{CO}[c] (s^{-1})	0.018	0.029	0.019
k_{C^*}[c] (s^{-1})	0.061	0.060	0.061
N_{C^*}/N_{CO}[b,c]	0.30	0.48	0.33
Wet/dry ratios[c]			
CH_4 selectivity	—	0.40	—
Ethene fraction in C_2	—	4.1	—
k_{CO}	—	1.55	—
k_{C^*}	—	0.99	—
N_{C^*}/N_{CO}	—	1.52	—

[a] Partial pressures in bar as $P(H_2) : P(CO) : P(H_2O)$; $T = 210°C$.
[b] Carbon-based selectivity.
[c] Uncertainty in absolute rate values, ±25%; uncertainty in relative values (ratios and adsorbed CO), ±10%.

Unsupported Co–Re Catalyst

Table 3 summarizes the results on the unsupported Co–Re catalyst. These results, obtained at industrially relevant high syngas pressures, reflect both reversible and irreversible changes during the water cofeed experiments. The data from the wet runs are tabulated under the results from the corresponding dry runs. These wet/dry experimental pairs were run at the same condition, except that the cofed water was replaced by an inert gas in the dry runs. The experiments are listed from left to right in the time sequence of the wet runs to track the irreversible changes in catalyst properties (vide infra). The corresponding dry results, all obtained before the water cofeeding sequence, are placed immediately above the wet-feed runs in the table, but they are not in time sequence.

The periodic activity checks at standard conditions (10 bar H_2, 5 bar CO, 8 bar inert, 220°C, and 11 ± 2% CO conversion; see Experimental) showed no measurable change to the catalyst during the entire sequence of dry experiments, which included changes in temperature and syngas composition (39). The averaged results from the activity checks during the dry experiments are shown in the first column among the dry results. They represent the properties of the catalyst just prior to the steam addition experiments and are also duplicated in the first column of the wet results. Changes are evident in the activity check (run 33) performed after the first three water cofeed runs (30–32) all with 4 bar of water. Further changes are evident in the activity check (run 38) after run 37, the water cofeed experiment with 8 bar of water. Since the catalyst showed irreversible changes during the water cofeeding experiments, a final activity check (run 39) was performed after regenerating the catalyst in 250°C hydrogen at 20 bar for 2 h to see if the original catalyst performance could be recovered. The activity check results obtained before and during the water cofeeding sequence are all shown in the shaded columns in Table 3. The irreversible effects of water are described next so that the reversible effects of water addition may be more clearly defined.

Irreversible effects of water on the unsupported catalyst. Since all measured kinetic and selectivity parameters are affected by reaction conditions, the irreversible changes in catalyst properties are tracked by the activity check results, all performed at identical reaction conditions. The activity checks shown in Fig. 3 demonstrate the progressive changes in the catalyst during the water cofeeding experiments from

TABLE 3

Kinetic and Selectivity Results for the Unsupported Co–Re Catalyst

		Run					
	AC[a]	25	18	6	8	11	Error[b]
Results from dry-feed experiments							
Feed partial pressures[c]	10:5:0	10:2.5:0	5:1.25:0	5:2.5:0	8:4:0	2:1:0	
CH_4 selectivity	0.069	0.145	0.156	0.064	0.063	0.140	10%
CO_2 selectivity	0.01	0.006	0.011	0.011	0.011	0.015	40%
C_{8+} selectivity	0.756	0.644	0.601	0.774	0.773	0.552	5%
f_{alkene} (C_2–C_7)	0.68	0.49	0.53	0.70	0.70	0.56	5%
r'_{CO} (μmol CO/mol Co s^{-1})	222	285	167	197	211	76	6%
N_{CO}/N_{Co}	0.0032	0.0028	0.0031	0.0030	0.0031	0.0029	5%
k_{CO} (s^{-1})	0.072	0.092	0.054	0.064	0.069	0.024	10%
k_{C^*} (s^{-1})	0.110	0.146	0.141	0.110	0.099	0.071	12%
N_{C^*}/N_{CO}[d]	0.654	0.631	0.381	0.576	0.688	0.339	15%

		Run							
	AC[a]	30	31	32	33	36	37	38	39
Results from water cofeed experiments and standard condition activity checks									
Feed partial pressures[c]	10:5:0	10:2.5:4	5:1.25:4	5:2.5:4	10:5:0	8:4:2	2:1:8	10:5:0	10:5:0
CH_4 selectivity	0.069	0.068	0.101	0.040	0.063	0.044	0.031	0.083	0.059
CO_2 selectivity	0.01	0.022	0.026	0.028	0.009	0.014	0.086	0.01	0.007
C_{8+} selectivity	0.756	0.754	0.678	0.822	0.733	0.812	0.775	0.710	N/A
f_{alkene}(C_2–C_7)	0.68	0.66	0.86	0.73	0.69	0.72	0.78	0.67	N/A
r'_{CO} (μmol CO/mol Co s^{-1})	222	240	237	178	147	182	52	64	134
N_{CO}/N_{Co}	0.0032	0.0029	0.0025	0.0025	0.0031	N/A	0.0017	0.0022	0.0022
k_{CO} (s^{-1})[d]	0.072	0.078	0.077	0.058	0.048	N/A	0.024	0.030	0.060
k_{C^*} (s^{-1})	0.110	0.103	0.095	0.070	0.068	N/A	0.035	0.049	0.087
N_{C^*}/N_{CO}[d,e]	0.654	0.745	0.790	0.800	0.695	N/A	0.627	0.601	0.689

Note. All runs at 210°C. Shaded columns contain data from activity checks at standard conditions.

[a] Average results of activity checks (AC) at standard condition with fresh catalyst before wet runs.

[b] Average percentage error in the row parameter (also applies to water cofeed conditions).

[c] Partial pressures in bar as $P(H_2):P(CO):P(H_2O)$.

[d] N_{C^*} calculated using CO conversion rates on a CO_2-free basis.

[e] To correct for the cobalt site counting error from the competitive adsorption of water in the wet runs, values were calculated for runs 30–32 and 37 using N_{CO}/N_{Co} from activity checks 33 and 38, respectively.

Table 3. These values show the $k_{C^*}/(k_{C^*}$ fresh), $k_{CO}/(k_{CO}$ fresh), and $N_{CO}/(N_{CO}$ fresh) ratios.

Irreversible changes in the catalyst properties first show up after the three water cofeeding experiments (runs 30–32) with 4 bar of steam. Although in activity check 33 the amount of adsorbed CO does not change, both k_{C^*} and k_{CO} decrease by approximately the same fraction (33–38%). In activity check 38, immediately after the 8-bar water cofeeding run (run 37), not only is there a further proportional decrease in both k_{C^*} and k_{CO}, to 40% of their original value, but the CO inventory also decreases by approximately 35%. As shown in activity check 39, hydrogen treatment recovers most (80%) of the site activity, measured by k_{C^*} and k_{CO}, but does not recover the original number of CO adsorption sites. We attribute this permanent 35% inventory loss of adsorbed CO to cobalt surface loss due to sintering. Sintering of this unsupported cobalt catalyst apparently is facilitated by the high (>4 bar) steam partial pressure. It is interesting that Holmen and co-workers (18, 19) also observed a reduction in the number of cobalt sites of their alumina-supported catalyst upon steam treatment. However, there was no loss in site activity under the conditions of their study.

Despite the observed activity loss, the N_{C^*}/N_{CO} ratio in the activity checks before and after the water cofeeding sequences remains unchanged (see N_{C^*}/N_{CO} values in the shaded columns of Table 3). This is the direct consequence of the parallel and proportional reduction of k_{C^*} and k_{CO} upon deactivation (see our earlier discussion of the dynamic balance of active intermediates on the catalyst surface). It is significant that just as N_{C^*}/N_{CO} is not affected, the selectivity parameters are not much affected either, which indicates that the key branching ratios in the hydrocarbon synthesis mechanism are also largely unaffected as the

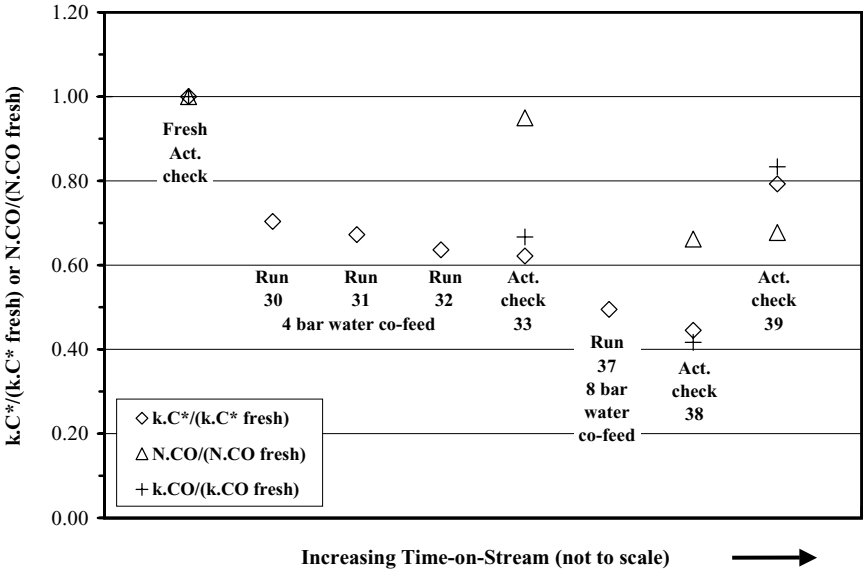

FIG. 3. Changes to the unsupported catalyst during the water cofeed experiments shown in Table 3. Periodic activity checks performed at $P(H_2):P(CO) = 10:5$. The data represent the ratio of k_{C^*} in the water cofeeding experiments to that measured in the relevant dry experiment. See text for discussion.

catalyst deactivates. The mechanistic implications of these facts are discussed later in connection with our proposed selectivity model.

Reversible effects of water. As we stated earlier, quantifying the reversible effects of water requires the separation of reversible and irreversible effects that occurred during water cofeeding. Since the dry control experiments (6, 8, 11, 18, and 25) were not performed immediately after the water cofeed experiments, we have to correct them for the irreversible changes caused by deactivation. We can base these corrections on the activity check results. Since dry conditions, such as those used in activity checks, did not induce measurable deactivation, and since the wet condition data were collected right before switching to activity checks, this method is straightforward for runs 32 and 37. First, a hypothetical set of dry results is calculated by linearly extrapolating the measured data to the deactivated state of the corresponding wet runs. The correction factors can be derived from the changes observed in the bracketing activity checks. Thus, for example, the corrected k_{CO} value for run 6 is calculated by multiplying the measured value ($0.064\ s^{-1}$) by the k_{CO} ratio (0.63) from experiment 33 and the average of the activity checks prior to run 30. This correction yields an adjusted k_{CO} value of $0.40\ s^{-1}$ in run 6. A comparison of this with the measured value of $0.58\ s^{-1}$ in water cofeed experiment 32 suggests that water under these conditions reversibly increases k_{CO} by a factor of 1.45 (=0.58/0.40). Without the separation of the reversible and irreversible effects, the raw numbers would only show a mild overall decrease in k_{CO}. Similar calculations can be performed for the other parameters in run 6 and for the 37/11 wet/dry run pair. The thus-calculated kinetic parameters now can be used to determine the reversible kinetic effects of water.

The separation of reversible and irreversible effects of water in runs 30 and 31 needs some further consideration. In this regard, an analysis of the k_{C^*} values is instructive. First, recall that k_{C^*} for the supported catalyst was not affected by the presence of water (see Table 2). Furthermore, the results of dry experiments listed in Table 3 suggest that k_{C^*} values at elevated total syngas pressures are the same within experimental error as long as the $H_2:CO$ ratios are the same (compare k_{C^*} in runs 18 and 25 or runs 6 and 8 and the average of fresh activity checks). Since neither the surface inventory of CO nor k_{C^*} changed during run 31 as compared to the end of run 30, we can conclude that no significant irreversible changes occurred in run 31. The nature and degree of irreversible changes in run 30 can be best estimated from the trend of the wet/dry k_{C^*} ratios plotted in Fig. 3. Based on the analysis of the results with the supported catalyst (see Table 2), the wet/dry ratio of k_{C^*} should be equal to one if all parameters, except for the water partial pressure, are the same. As depicted in Fig. 3, k_{C^*} in run 30 drops 40% compared both to run 25 and to the preceding activity check, indicating a 40% activity loss. In fact, an inspection of the wet/dry k_{C^*} ratios in the first standard condition activity check and runs 30–33 suggest that nearly all the accumulated site activity loss up to run 33 takes place during the first wet run, number 30. This also means that cobalt site activity loss happens relatively fast upon an increase in water partial pressure to 4 bar but the site activity then stabilizes. It should also be noted that

TABLE 4

Reversible Water Effects on the Unsupported Co Catalyst: Ratios of Wet/Dry Results

	Wet/dry runs				
	30/25	31/18	32/6	36/8	37/11
Feed partial pressures[a]	10:2.5:4/ 10:2.5:0	5:1.25:4/ 5:1.25:0	5:2.5:4/ 5:2.5:0	8:4:2/8:4:0	2:1:8/2:1:0
CH_4 selectivity	0.47	0.65	0.63	0.70	0.22
$f_{alkene}(C_2–C_7)$	1.35	1.62	1.04	1.03	1.39
k_{CO}	1.3	2.1	1.4	—	2.5
k_{C^*}	1.1	1.0	1.0	—	1.2
N_{C^*}/N_{CO}	1.18	2.07	1.39	—	1.85

[a] Partial pressures in bar as $P(H_2):P(CO):P(H_2O)$; all runs at 210°C.

the site activity drop in run 32 based on the wet/dry ratios is identical to the drop based on the run 33/fresh activity check ratio, confirming the validity of the previous arguments.

Table 4 summarizes the reversible kinetic and selectivity effects of water as ratios of the corresponding wet/dry parameters obtained after performing the corrections as described above. From the results in the table we can observe the following surface inventory and kinetic effects of water on the unsupported Co–Re catalyst.

1. The surface CO inventory is relatively constant upon water addition, except for the irreversible site loss that accompanied run 37. The small 10–20% decrease during runs 30–32 at 4 bar water pressure may signal competitive water adsorption reaching detectable levels. None of the permanent decrease in N_{CO}/N_{Co} that occurs during run 37 at 8-bar feed water partial pressure is recovered after hydrogen treatment. The irreversibility suggests cobalt site loss is most likely due to sintering.

2. The surface concentration of active carbon (N_{C^*}/N_{CO}) increases substantially in the presence of water in all cases. It should be noted that catalyst deactivation does not influence this conclusion since N_{C^*}/N_{CO} does not change in activity checks even after the irreversible changes of the catalyst.

3. The as-measured wet/dry k_{CO} values do not show a clear trend when no attempt is made to correct for the irreversible deactivation process. However, when the corrections described above are made, substantial increases, similar to that seen with the supported catalyst, can be seen.

4. The raw k_{C^*} numbers indicate a decrease in the reactivity of the C* pool. However, after correcting for the irreversible changes, no difference in the value of k_{C^*} is observed between wet and dry runs. This, of course, is anticipated by the results in Fig. 3 and is in agreement with the results on the titania-supported catalyst. Also, just as in the case of the titania-supported catalyst, the shape of the measured methane transients follows a single exponential decay (see Fig. 2), suggesting a homogeneous pool of surface carbon intermediates (31).

Selectivity effects of water mirror those on the supported catalyst and those previously published (1, 2, 13). These trends are not subject to uncertainty due to catalyst deactivation, since activity checks performed under standard conditions did not reveal any significant changes in the selectivity parameters either. Figure 4 shows the wet/dry selectivity ratios of the $C_1–C_7$ and C_{8+} products for two syngas compositions in Table 3. The C_{8+} selectivity increases, while

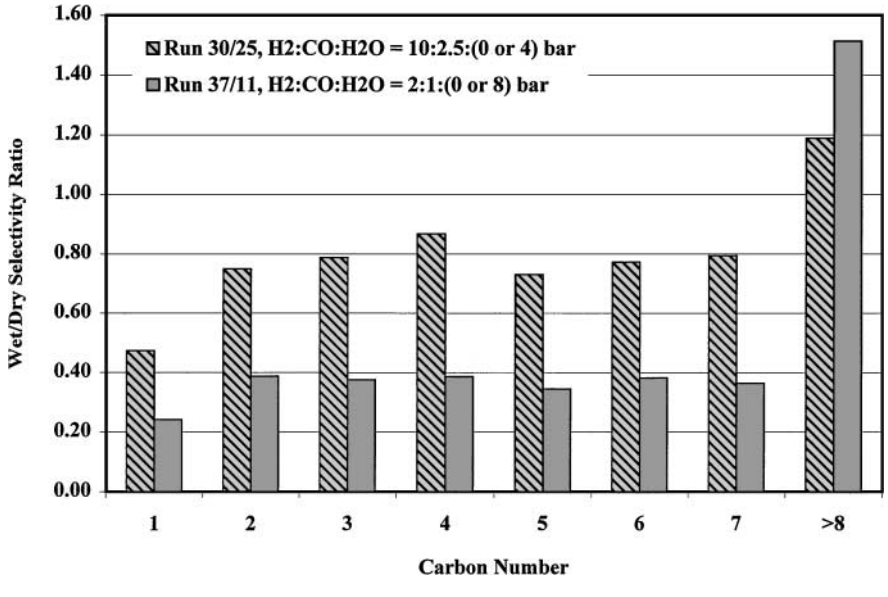

FIG. 4. Selectivity changes upon addition of water: Wet/dry ratios of carbon-based selectivity (CO_2-free basis) for two representative experiment pairs shown in Table 2.

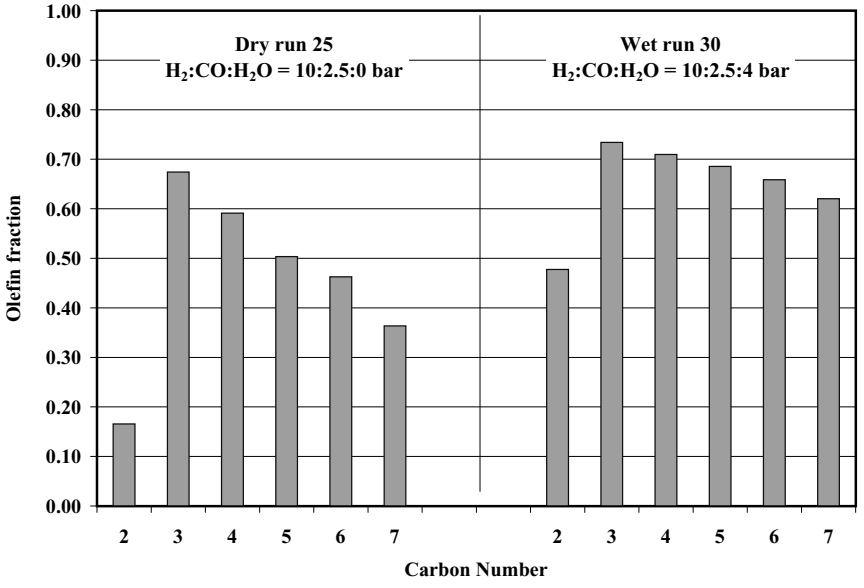

FIG. 5. Alkene and alkane selectivity values under dry (run 25) and wet (run 30) conditions. $P(H_2) : P(CO) : P(H_2O) = 10 : 2.5 : (0 \text{ or } 4)$.

selectivity for lower carbon number products decreases upon water addition. The decrease in methane selectivity during water cofeeding is particularly noticeable. Clearly, water increased the probability of chain propagation, ASF α, in our fixed-bed tests. The increase in α is larger at higher water partial pressures. The olefin fractions in the C_2–C_7 products also increase upon water addition (compare the olefin fractions for run 30 with 4 bar of steam with its companion dry run, 25, in Fig. 5). The well-documented (1) decreasing olefinicity with increasing carbon numbers is quite obvious at dry conditions in Fig. 5, but in the presence of cofed water, this tendency decreases. This phenomenon indicates that secondary hydrogenation of olefins to paraffins is inhibited by water, most likely due to competition with hydrogen adsorption.

DISCUSSION

Our isotope transient experiments reveal, for the first time, the simultaneous changes in overall activity and selectivity as well as the changes in surface composition upon addition of water in cobalt-catalyzed FT synthesis. These changes are part of the intrinsic mechanism on cobalt since they occur on an unsupported catalyst. One of the major trends in the isotope transient data in Tables 2 and 3 is that water addition causes an increase in the surface inventory of active carbon at all the syngas compositions studied. The data also reveal that this trend is caused by an increase in the rate of carbon monoxide activation without a parallel increase in the reactivity of the active carbon intermediates.

The resultant "crowding" of the surface by active carbon intermediates is associated with reversible changes in selectivity. Correlating, for example, methane selectivity and surface carbon inventory can test the connection of surface concentration of active carbon and product selectivity. Figure 6 shows methane selectivity as a function of the surface concentration of active carbon from Tables 2 and 3 for the experiments with $H_2 : CO$ ratios of 2. The graph clearly demonstrates the trend of decreasing methane selectivity at increased active carbon inventory levels and that a continuous trend is observed as long as the $H_2 : CO$ ratio is constant. Figure 7 shows similar behavior for the two experiments with $H_2 : CO$ ratios of 4, but the methane selectivity at a given surface carbon coverage is higher than that observed in the $H_2 : CO = 2$ series shown in Fig. 6. These regular trends imply that carbon coverage is a dominant parameter governing selectivity at a given temperature as long as the $H_2 : CO$ ratio is held constant.

In a previous study (36), we noticed a similar trend (although smaller changes) among a group of catalysts studied under identical reaction conditions. A considerable variation in methane selectivity was observed but this variability did not correlate with such catalyst parameters as the nature of support, Co loading, or the presence of Re promoter. While there was no apparent correlation with catalyst composition, a correlation appeared to link decreased methane selectivity to higher surface coverage of active carbon in a manner similar to that observed in Figs. 6 and 7. A simple, modified Flory model was able to reproduce the covariation seen in these experiments. It contains the intuitively appealing feature that methane formation has a lower effective reaction order in monomer coverage than does higher hydrocarbon formation. We show below that a similar explanation can hold for the more dramatic changes in selectivity seen for water addition.

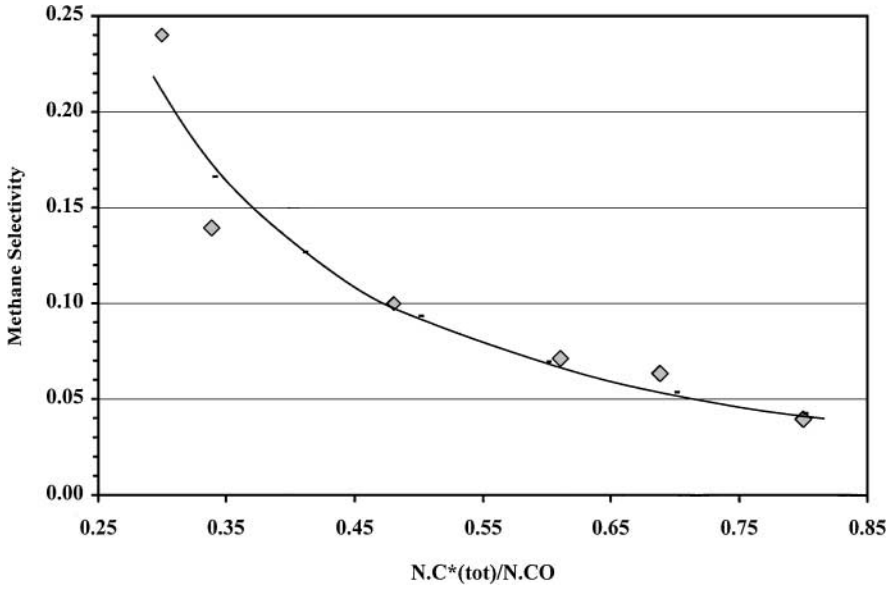

FIG. 6. Methane selectivity plotted against surface active carbon coverage for the experiments shown in Tables 2 and 3 with $H_2 : CO = 2 : 1$. Solid line: The model described in the text with $k_g/k_{tn} = 12.2$, $k_{t1}/k_{tn} = 5.1$.

Monomer Crowding Effects on Selectivity

The scheme in Fig. 8 shows a modified polymerization mechanism for hydrocarbon synthesis. In the scheme the rate laws for each step in the process are adjacent to the relevant arrow. These contain explicit dependencies only on the C* coverage, but of course the rate coefficients contain hidden dependencies on other parameters, such as, for example, H* coverage and thus H_2 pressure. Methane formation is given a termination rate constant, k_{t1}, distinct from those for the C_{2+} surface species, k_{tn}. Qualitatively, it is easy to see from this mechanism that the production of higher hydrocarbons should have a higher effective reaction order in θ_{C^*} than methane formation, since the monomer is involved both in the initiation and in the growth of higher hydrocarbons. This model is quite primitive and cannot capture many of the finer details of the product distribution better addressed by other models (1, 41–43). Nevertheless, it captures the essence of the interdependence of monomer coverage and selectivity. The quantitative prediction of this

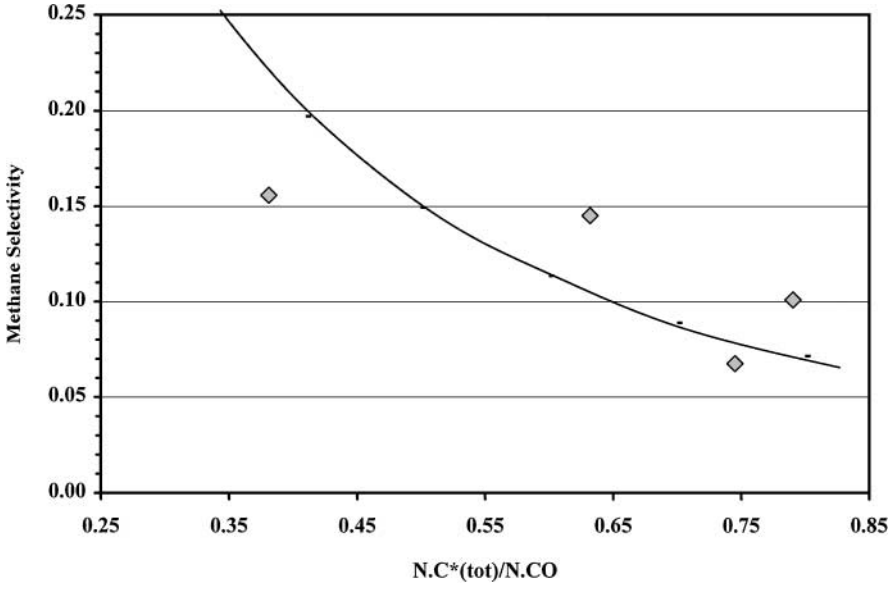

FIG. 7. Methane selectivity plotted against surface active carbon coverage for the experiments shown in Table 3 with $H_2 : CO = 4 : 1$. Solid line: The model described in the text with $k_g/k_{tn} = 9.8$, $k_{t1}/k_{tn} = 5.9$.

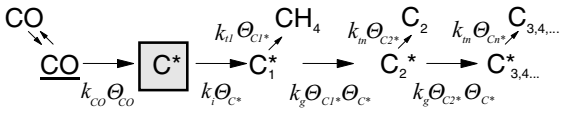

FIG. 8. Kinetic pathways for the flow of active carbon based on a simple Flory polymerization mechanism.

model for methane selectivity can be calculated by applying the steady state condition to the intermediates and performing the summation over the C_{2+} product distribution. The result is the expression

$$S(CH_4) = \{1 + (k_g/k_{t1})\theta_{C^*}[2 + (k_g/k_{tn})\theta_{C^*}]\}^{-1}, \quad [7]$$

where k_g is the chain propagation rate constant. According to this expression methane selectivity will decrease as θ_{C^*} increases even if the ratios of rate constants within the hydrocarbon synthesis network remain constant. In fact, for large values of the propagation/termination ratios (k_g/k_{t1}) and (k_g/k_{tn}), methane selectivity should approximately decrease as $\theta_{C^*}^{-2}$. The trend predicted by this model with a particular set of rate coefficient ratios is compared with our methane selectivity data in Fig. 6 (model prediction is the solid line).[2] The values of θ_{C^*} for the model are calculated by assuming that the active sites are saturated by adsorbed CO, i.e., by giving θ_{CO} in the relevant dry experiments the value of one (i.e., $N_{C^*}/N_{CO,dry} = \theta_{C^*}$). This is reasonable in view of the constant value of θ_{CO} over all of the dry conditions and only minor changes in θ_{CO} in the presence of water. The trends in the model are not sensitive to this convention, since anything proportional to θ_{C^*} will reproduce the trend shown in Fig. 6 with appropriate rate coefficients. The model parameters used in the calculation are given in the figure captions. The rate coefficient values themselves are expected to depend on the gas composition, but the single trend obtained at different total syngas pressures implies that the propagation/termination ratios are governed primarily by the $H_2:CO$ ratio rather than by the value of either partial pressure alone. In Fig. 7, the results at higher $H_2:CO$ ratios are fit with the same model, but with a different set of model parameters. The need for a different set of model parameters arises from the fact that methane selectivity depends not only on θ_{C^*} but also on the propagation/termination rate ratios. Not surprisingly, the $H_2:CO$ ratio strongly influences the latter and thus needs to be kept constant in order to obtain a good selectivity–θ_{C^*} correlation. It is remarkable that holding the $H_2:CO$ ratio constant is sufficient to isolate the θ_{C^*} dependence. We also recognize that our simple model does not account for a number of other variables that may play a role in governing product selectivity. However, our results suggest that θ_{C^*} and the propagation/termination rate ratios exert such an overwhelming effect that one can predict FT selectivity at an acceptable accuracy as long as these two factors are accounted for.

In addition to predicting lower methane selectivity, the model also predicts that higher chain growth probability should arise from increased θ_{C^*}:

$$\alpha = k_g\theta_{C^*}/(k_g\theta_{C^*} + k_{tn}). \quad [8]$$

Such a general trend is seen in the α values derived from the $C_{8+}/(C_5–C_7)$ ratios, as shown in Fig. 9. The model prediction is consistent with this trend.

The changes in selectivity associated with the addition of water can thus be well represented as being a by-product of an increase in the active carbon coverage. The increase in C* coverage is caused by an increase in CO reactivity without a parallel increase in the overall reactivity of C*. This, in turn, causes a "traffic jam" on the surface and the inherent carbon coverage dependence in the FT mechanism produces the selectivity changes. While the data indicate that water has little effect on k_{C^*}, the overall reactivity of the active carbon pool, it must be remembered that k_{C^*} is a composite rate coefficient representing the entire hydrocarbon synthesis network. From the model in Fig. 9, the following expression can be derived for k_{C^*}:

$$k_{C^*} = k_i\{(k_g\theta_{C^*}/k_{tn} + 1)^{-1} + (k_g\theta_{C^*}/k_{tn} + 2)(k_g\theta_{C^*}/k_{tn} + 1) \times (k_g\theta_{C^*}/k_{tn} + k_{t1}/k_{tn})^{-1}\}. \quad [9]$$

This expression shows a dependence of k_{C^*} on θ_{C^*} that reduces to be approximately proportional to the rate of initiation, $k_i\theta_{C^*}$, for large values of k_g/k_{tn}. Therefore, the fact that k_{C^*} does not change while θ_{C^*} increases upon the addition of water actually implies, according to this simple model, that water causes a decrease in the initiation rate coefficient, k_i. The lower probability of initiating hydrocarbon chains is effectively offset by the increased rate of monomer consumption, building higher molecular weight products.

The increase in CO reactivity in the presence of water could arise from a variety of mechanisms. The most obvious is a direct interaction between coadsorbed CO and water that lowers the barrier to CO dissociation. There is persistent evidence in the surface science literature of a significant interaction of CO and coadsorbed water on a variety of transition metal surfaces (44–51). In general, a significant lowering of the CO vibrational frequency, either by shifts or by the appearance of new bands, accompanies the coadsorption of water. Both direct adsorbate–adsorbate (e.g., weak hydrogen bonding of water to the oxygen of CO) (44–51) and metal-mediated mechanisms (e.g., increased backbonding into the CO π^* orbital) (44–51) have been proposed as explainations for the interaction. Other possibilities include the oxidation of low-coordination sites, or the reconstruction of the surface in the presence of water.

[2] In comparing the model predictions with the data we should mention that the experimental values represent averages over the catalyst bed.

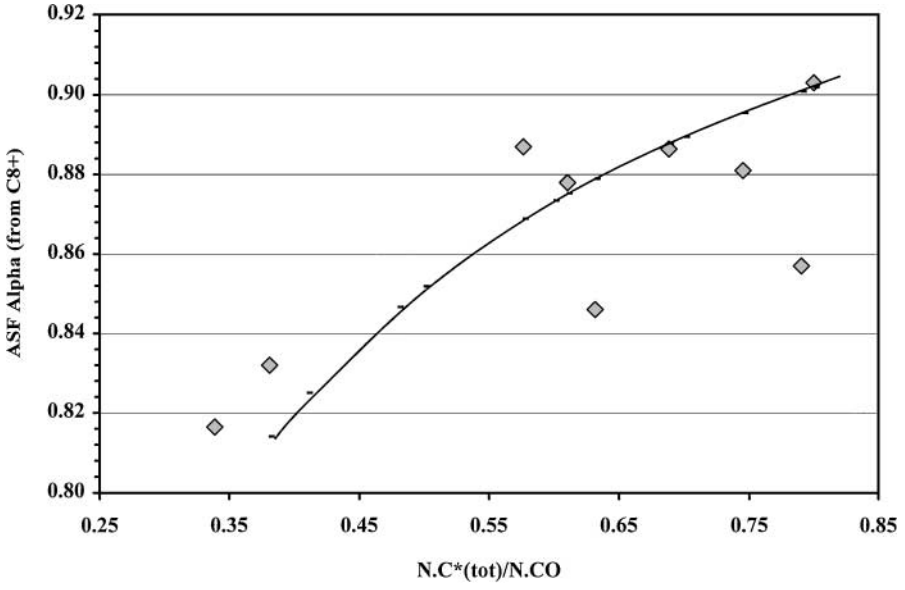

FIG. 9. Higher hydrocarbon growth probability vs surface C* coverage. Chain growth probability, α, is obtained from a Flory distribution required to produce the measured $C_{8+}/(C_5–C_7)$ selectivity ratio. Solid line: The prediction of the polymerization model with $k_g/k_{tn} = 11.5$.

In any case, all are plausible, since only a 3 kJ/mol change in the activation energy for dissociation at this temperature would result in a twofold increase in the reaction rate. The decrease in at least one of the fundamental rate constants in the hydrocarbon synthesis network is also indicated and could be the result of decreased hydrogen availability, as has been previously proposed (1, 13).

There is a striking similarity between the effects of water as seen here on cobalt and earlier results reported by Komaya *et al.* on the effects of TiO_x fragments on the low-pressure hydrogenation of CO with silica-supported ruthenium catalysts (52). The isotopic transient data in their study revealed that TiO_x fragments increased the CO activation rate and decreased the rate coefficients of the hydrocarbon synthesis pathways. The resulting increase in surface carbon monomer inventory caused lower methane selectivity and higher chain growth probability. The increase in CO activation rate was attributed to a direct interaction between CO and the Lewis acid site of the TiO_x fragments, which would weaken the C–O bond. One might suggest that adventitious inorganic contaminants could serve as CO dissociation "promoters" and thus cause much of the variability of the CO turnover frequency and methane selectivity values noted in our previous study (35, 36).

We should point out that olefin readsorption from the liquid phase in the catalyst pores holds the potential for contamination of the surface monomer pool (53–58) since chain growth is partly reversible (56). A significant amount of this exchange with a large pool of products in the liquid phase, although unlikely, would result in overcounting the surface monomer concentration. Without direct measurements of this effect, some uncertainty will remain in the interpretations of these and other isotope transient experiments under FT conditions.

SUMMARY AND CONCLUSIONS

1. CO inventory on cobalt FT catalysts is essentially constant in a wide range of industrially relevant syngas pressures, indicating surface saturation in CO.

2. Water cofeeding does not significantly affect CO inventory even at syngas pressures of a few bars. Water apparently does not compete effectively with CO for the cobalt surface.

3. Water addition at partial pressures up to 8 bar to a functioning unsupported cobalt FT catalyst increases the reactivity of adsorbed CO on the surface without changing the reactivity of the active surface carbon intermediate. This in turn leads to increased surface concentration of the monomeric carbon precursors to hydrocarbon formation.

4. A decrease in methane selectivity and an increase in ASF α are observed in the presence of increased water partial pressure. These selectivity changes correlate with increased surface concentration of active carbon caused by increased water partial pressure.

5. Simple "surface crowding" kinetic models can explain the simultaneous increase in surface carbon concentration and decrease in methane selectivity.

6. Product olefinicity becomes less dependent on carbon number upon water cofeeding. Water inhibits the secondary hydrogenation of the primary olefin products, likely as a result of competitive adsorption by water.

7. Water deactivates unsupported cobalt catalysts at high partial pressures. The deactivation accompanies

reduced site activity and/or lower CO surface inventory. While hydrogen treatment largely recovers site activity, it does not affect surface inventory. The latter observation suggests cobalt surface loss due to sintering. This sintering process is greatly facilitated by high (>4 bar) water partial pressure.

ACKNOWLEDGMENTS

The authors gratefully acknowledge the generous supply of catalyst samples by Dr. Andre Malek and Dr. Charles H. Mauldin and the technical assistance of Mr. Gregory J. DeMartin in constructing the high-pressure transient kinetic unit, all of ExxonMobil Research and Engineering Co. CAM and CJB thank ExxonMobil Research and Engineering Co. for research support.

REFERENCES

1. Iglesia, E., *Appl. Catal. A* **161**, 59 (1997).
2. Schulz, H., Claeys, M., and Harms, S., *Stud. Surf. Sci. Catal.* **107**, 193 (1997).
3. Iglesia, E., *in* "Proceedings XV Iberoamerican Catal. Symp., Plenary Address" (E. Herrero, O. Anunziata, and C. Perez, Eds.), PL-17 (1996).
4. Schulz, H., van Steen, E., and Claeys, M., *Stud. Surf. Sci. Catal.* **81**, 455 (1994).
5. Withers, H. P., Eliezer, K. F., and Mitchell, J. W., *Ind. Eng. Chem. Res.* **29**, 1807–1814 (1990).
6. Kim, C. J., U.S. Patent 5,227,407 (1993).
7. Kim, C. J., European Patent 0,355,218 (1990).
8. Kim, C. J., European Patent 0,339,923 (1989).
9. Iglesia, E., and Madon, R., U.S. Patent 4,754,092 (1988).
10. Minderhoud, J. K., Post, M. F. M., Sie, S. T., and Sudholter, S. T. S., U.S. Patent 4,628,133 (1986).
11. Yates, I. C., and Satterfield, C. N., *Energy Fuels* **5**, 168 (1991).
12. Zennaro, R., Tagliabue, M., and Bartholomew, C. H., *Catal. Today* **58**, 309 (2000).
13. Hilmen, A. M., Lindvag, O. A., Bergene, E., Schanke, D., Eri, S., and Holmen, A., *Stud. Surf. Sci. Catal.* **136**, 295 (2001).
14. van Berge, P. J., van de Loosdrecht, J., Barradas, S., and van der Kraan, A. M., *Catal. Today* **58**, 321 (2000).
15. van Berge, P. J., van de Loosdrecht, J., Barradas, S., and van der Kraan, A. M., *in* "ACS Div. of Petroleum Chem. Preprints, 217th ACS Natl. Mtg., Anaheim, CA," p. 84. Am. Chem. Soc., Washington, DC, 1999.
16. Gottschalk, F. M., Copperthwaite, R. G., van der Riet, M., and Hutchings, G. J., *Appl. Catal.* **38**, 103 (1988).
17. Hilmen, A. M., Schanke, D., Hanssen, K. F., and Holmen, A., *Appl. Catal. A* **186**, 169 (1999).
18. Rothaemel, M., Hanssen, K. F., Blekkan, E. A., Schanke, D., and Holmen, A., *Catal. Today* **38**, 79 (1997).
19. Hanssen, K. F., Blekkan, E. A., Schanke, D., and Holmen, A., *Stud. Surf. Sci. Catal.* **109**, 193 (1997).
20. Schanke, D., Hilmen, A. M., Bergene, E., Kinnari, K., Rytter, E., Adnanes, E., and Holmen, A., *Energy Fuels* **10**, 867 (1996).
21. Schanke, D., Hilmen, A.M., Bergene, E., Kinnari, K., Rytter, E., Adnanes, E., and Holmen, A., *in* "ACS Div. of Fuel Chem. Preprints, 209th ACS Natl. Mtg., Anaheim, CA," Vol. 40, p. 167. Am. Chem. Soc., Washington, DC, 1995.
22. Schanke, D., Hilmen, A. M., Bergene, E., Kinnari, K., Rytter, E., Adnanes, E., and Holmen, A., *Catal. Letters* **34**, 269 (1995).
23. Zhang, Y., Wei, D., Hammache, S., and Goodwin, J. G., Jr., *J. Catal.* **188**, 281 (1999).
24. Kogelbauer, A., Weber, J. C., and Goodwin, J. G., Jr., *Catal. Lett.* **34**, 259 (1995).
25. Shannon, S. L., and Goodwin, J. G., Jr., *Chem. Rev.* **95**, 677 (1995).
26. van Dijk, H. A. J., Hoebink, J. H. B. J., and Schouten, J. C., *Chem. Eng. Sci.* **56**, 1211 (2001).
27. van Dijk, H. A. J., Ph.D. thesis. Technische Universiteit Eindhoven, Eindhoven, Holland, 2001.
28. Rohr, F., Lindvag, O. A., Holmen, A., and Blekkan, E. A., *Catal. Today* **58**, 247 (2000).
29. Khodadadi, A. A., Hudgins, R. R., and Silveston, P. L., *Can. J. Chem. Eng.* **76**, 239 (1998).
30. Belambe, A. R., Oukaci, R., and Goodwin, J. G., Jr., *J. Catal.* **166**, 8 (1997).
31. Biloen, P., Helle, J. N., van den Berg, F. G. A., and Sachtler, W. M. H., *J. Catal.* **81**, 450 (1983).
32. Mims, C. A., and McCandlish, L. E., *J. Phys. Chem.* **91**, 929 (1987).
33. Krishna, K. R., and Bell, A. T., *J. Catal.* **139**, 104 (1993).
34. Stockwell, D. M., Bianchi, D., and Bennett, C. O., *J. Catal.* **113**, 13 (1988).
35. Mims, C. A., and Bertole, C. J., *Stud. Surf. Sci. Catal.* **136**, 375 (2001).
36. Mauldin, C. H., and Varnado, D. E., *Stud. Surf. Sci. Catal.* **136**, 417 (2001).
37. Mims, C. A., Bertole, C. J., Kiss, G., and Joshi, P. V., *Stud. Surf. Sci. Catal.* **136**, 369 (2001).
38. Mauti, R., Ph.D. thesis. University of Toronto, Toronto, Canada, 1994.
39. Bertole, C. J., Ph.D. thesis. University of Toronto, Toronto, Canada, 2002.
40. van der Laan, G. P., and Beenackers, A. A. C. M., *Catal. Rev.–Sci. Eng.* **41**, 255 (1999).
41. van der Laan, G. P., and Beenackers, A. A. C. M., *Ind. Eng. Chem. Res.* **38**, 1277 (1999).
42. Schulz, H., and Claeys, M., *Appl. Catal. A* **186**, 91 (1999).
43. Nowicki, L., Ledakowicz, S., and Bukur, D. B., *Chem. Eng. Sci.* **56**, 1175 (2001).
44. Moyes, R. B., and Roberts, M. W., *J. Catal.* **49**, 216 (1977).
45. Peebles, D. E., and White, J. M., *Surf. Sci.* **144**, 512 (1984).
46. White, J. M., and Akhter, S., *Crit. Rev. Solid State Mater. Sci.* **14**, 131 (1988).
47. Ellis, T. H., Kruus, E. J., and Wang, H., *Surf. Sci.* **273**, 73 (1992).
48. Brosseau, R., Ellis, T. H., Morin, M., and Wang, H., *J. Electron Spectrosc. Relat. Phenom.* **5455**, 659 (1990).
49. Kizhakevariam, N., Jiang, X., and Weaver, M., *J. Chem. Phys.* **100**, 6750 (1994).
50. Yuzawa, T., Higashi, T., Kubota, J., Kondo, J. N., Domen, K., and Hirose, C., *Surf. Sci.* **325**, 2239 (1995).
51. Nakamura, M., and Ito, M., *Chem. Phys. Lett.* **335**, 170 (2001).
52. Komaya, T., Bell, A. T., Weng-Sieh, Z., Gronsky, R., Engelke, F., King, T. S., and Pruski, M., *J. Catal.* **150**, 400 (1994).
53. Pichler, H., and Schulz, H., *Chem.-Ing.-Tech.* **42**, 1162 (1970).
54. Kobori, Y., Yamasaki, H., Naito, S., Onishi, T., and Tamaru, K., *J. Chem. Soc. Faraday Trans.* 1473 (1982).
55. Yamasaki, H., Kobori, Y., Naito, S., Onishi, T., and Tamaru, K., *J. Chem. Soc. Faraday Trans.* 2913 (1981).
56. Mims, C., Krajewski, J., Rose, K., and Melchior, M. T., *Catal. Lett.* **7**, 119 (1990).
57. Iglesia, E., Reyes, S. C., Madon, R. J., and Soled, S. L., *Adv. Catal.* **39**, 221 (1993).
58. Schulz, H., and Claeys, M., *Appl. Catal. A* **186**, 71 (1999).